Ni^{2+} Block of $Ca_V3.1$ (α1G) T-type Calcium Channels

Carlos A. Obejero-Paz, I. Patrick Gray, and Stephen W. Jones

Department of Physiology and Biophysics, Case Western Reserve University, Cleveland, OH 44106

Ni^{2+} inhibits current through calcium channels, in part by blocking the pore, but Ni^{2+} may also allosterically affect channel activity via sites outside the permeation pathway. As a test for pore blockade, we examined whether the effect of Ni^{2+} on $Ca_V3.1$ is affected by permeant ions. We find two components to block by Ni^{2+}, a rapid block with little voltage dependence, and a slow block most visible as accelerated tail currents. Rapid block is weaker for outward vs. inward currents (apparent K_d = 3 vs. 1 mM Ni^{2+}, with 2 mM Ca^{2+} or Ba^{2+}) and is reduced at high permeant ion concentration (110 vs. 2 mM Ca^{2+} or Ba^{2+}). Slow block depends both on the concentration and on the identity of the permeant ion (Ca^{2+} vs. Ba^{2+} vs. Na^+). Slow block is 2–3× faster in Ba^{2+} than in Ca^{2+} (2 or 110 mM), and is ∼10× faster with 2 vs. 110 mM Ca^{2+} or Ba^{2+}. Slow block is orders of magnitude slower than the diffusion limit, except in the nominal absence of divalent cations (∼3 μM Ca^{2+}). We conclude that both fast and slow block of $Ca_V3.1$ by Ni^{2+} are most consistent with occlusion of the pore. The exit rate of Ni^{2+} for slow block is reduced at high Ni^{2+} concentrations, suggesting that the site responsible for fast block can "lock in" slow block by Ni^{2+}, at a site located deeper within the pore. In contrast to the complex pore block observed for $Ca_V3.1$, inhibition of $Ca_V3.2$ by Ni^{2+} was essentially independent of voltage, and was similar in 2 mM Ca^{2+} vs. Ba^{2+}, consistent with inhibition by a different mechanism, at a site outside the pore.

INTRODUCTION

Many ions block channels by binding within the pore, preventing flux of permeant ions. In particular, several di- and trivalent cations bind with high affinity to the ion selectivity filter of voltage-dependent cation channels. Indeed, that is how calcium itself blocks permeation of monovalent cations, introducing calcium selectivity into a channel that has a high intrinsic conductance for monovalent cations (Almers et al., 1984; Hess and Tsien, 1984). High affinity blockers, which can block not only flux of monovalent cations but also current carried by calcium ions, have been especially useful as probes for the functional architecture of the calcium channel pore (Yang et al., 1993; Obejero-Paz et al., 2004).

Although the fundamental mechanism of ion selectivity is conserved among the Ca_V family of voltage-dependent calcium channels, it has long been recognized that there are significant quantitative differences in selectivity for permeation and block. Ni^{2+} has received particular attention. Originally thought to be a selective blocker of T-type calcium channels (Narahashi et al., 1987; Hagiwara et al., 1988), it is now clear that only one of the three cloned mammalian T-channels, $Ca_V3.2$, is strongly inhibited by Ni^{2+} (Lee et al., 1999), while one high voltage-activated channel, $Ca_V2.3$, is quite sensitive to Ni^{2+} (Soong et al., 1993). However, it has been suggested that Ni^{2+} acts in part by binding to a site on the extracellular side of the channel, affecting current through the channel allosterically, not only by binding within the permeation pathway itself (Zamponi et al., 1996). Lacinova et al. (2000) reported that Ni^{2+} accelerated deactivation of $Ca_V3.1$, interpreted as a modification of activation gating, but Diaz et al. (2005) concluded instead that this effect resulted from time-dependent block by Ni^{2+}.

Recently, mutational analysis has found that high affinity inhibition by Ni^{2+} of $Ca_V3.2$ requires a histidine near the extracellular side of the S4 transmembrane segment of domain I (Kang et al., 2005). Replacement of histidine with glutamine (the corresponding residue in $Ca_V3.1$) increased the IC_{50} from 5 to 300 μM in $Ca_V3.2$. The reverse mutation (Q172H in $Ca_V3.1$) had a partial effect, changing the IC_{50} from 300 to 60 μM. This suggests that high affinity inhibition by Ni^{2+} results from binding to an extracellular site (Kang et al., 2005). That result also reopens the question of the mechanism of the relatively low affinity inhibition of $Ca_V3.1$ by Ni^{2+}. One clue is that the effect of Ni^{2+} on $Ca_V3.2$ is essentially voltage independent (Diaz et al., 2005; Kang et al., 2005), while pore block by di- and trivalent cations is typically voltage dependent for Ca_V channels, including $Ca_V3.1$ (Lee et al., 1999; Serrano et al., 2000; Obejero-Paz et al., 2004).

We examine here not only the voltage dependence of Ni^{2+} inhibition of $Ca_V3.1$, but also the dependence on the chemical nature and the concentration of the

Correspondence to Stephen W. Jones: swj@case.edu

Abbreviation used in this paper: IIV, instantaneous current-voltage relationship.

The online version of this article contains supplemental material.

The Rockefeller University Press $30.00
J. Gen. Physiol. Vol. 132 No. 2 239–250
www.jgp.org/cgi/doi/10.1085/jgp.200809988

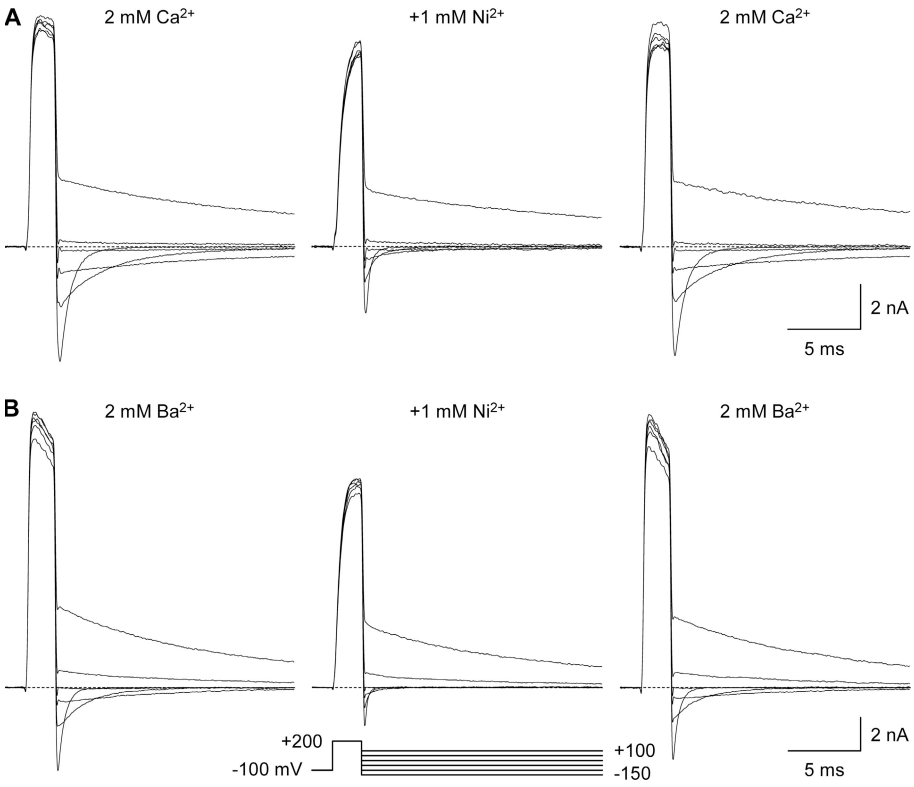

Figure 1. Effects of 1 mM Ni^{2+} on currents carried by 2 mM Ca^{2+} (A) or 2 mM Ba^{2+} (B), using the IIV protocol. Cells were depolarized from a holding potential of −100 to +200 mV for 2 ms, to activate the channels and relieve most inhibition by Ni^{2+}, followed by voltage steps in 10-mV increments from +100 to −150 mV for 100 ms. Only the initial portion of the tail currents is shown, for voltage steps in 50-mV increments. Records are shown before application of Ni^{2+} (left column), in 1 mM Ni^{2+} (middle column), and after washout of Ni^{2+} (right column). Dashed lines indicate zero current following leak subtraction. 3-kHz digital Gaussian filter. Cells b050825 (A), d051019 (B).

permeant ion. The potency of pore block is strongly influenced by competitive interactions among ions in the pore; for example, block is much stronger when monovalent ions are the charge carrier (Yang et al., 1993). We have also found that block by Mg^{2+} is considerably stronger in 2 mM Ba^{2+} than in 2 mM Ca^{2+} for $Ca_V3.1$, even though currents carried by Ba^{2+} and Ca^{2+} are quite comparable (Serrano et al., 2000). The nature of the ionic effects may vary among blocking ions, however, as the rate of block by Y^{3+} is sensitive to Ca^{2+} vs. Ba^{2+} for closed but not open channels (Obejero-Paz et al., 2004).

We report here that Ni^{2+} has two inhibitory effects on $Ca_V3.1$ channels, a rapid inhibition that is ion dependent but weakly voltage dependent, and a slower block (reflected in tail current acceleration) that is both ion and voltage dependent. Both effects are most consistent with interactions of Ni^{2+} with the ion conduction pathway, as opposed to an extracellular allosteric site (see Fig. S1, available at http://www.jgp.org/cgi/content/full/jgp.200809988/DC1). Ni^{2+} blocks $Ca_V3.1$ by mechanisms fundamentally different from the voltage-independent high-affinity block of $Ca_V3.2$.

MATERIALS AND METHODS

General methods for whole-cell patch clamp recording from HEK 293 cells stably transfected with $Ca_V3.1$ (α1G) were specified by Khan et al. (2008) and are only summarized here.

Experiments with $Ca_V3.2$ used transiently transfected HEK 293 cells. Cells were transfected at 80% confluence in 35-mm dishes using FuGENE6 (Roche) with 1.5 µg plasmid DNA encoding rat $Ca_V3.2$ and 0.5 µg CD8 pcDNA (gifts from E. Perez-Reyes [University of Virginia, Charlottesville, VA] and E. Ficker [Case Western Reserve University], respectively). One day after transfection, cells were dispersed with trypsin and transferred to coverslips. On the day of the experiment, usually 2 d after plating, transfected cells were identified using 1 µl Dynabeads CD8 (Dynal Biotech).

Pipet resistances were 1.8–2.3 MΩ. Access resistances in the whole-cell configuration were 5 ± 1 MΩ and were compensated by ∼90% ("correction") and ∼50% ("prediction"). Ni^{2+} was added in the concentrations indicated (as $NiCl_2$) without other change in the extracellular solution.

Effects of Ni^{2+} were examined by two basic protocols: the I-V protocol, where currents were recorded directly upon depolarization from a holding potential of −100 mV to the voltages indicated, and the IIV protocol, where the voltage was varied following a 2-ms step to +200 mV to maximally activate channels with minimal inactivation. These two protocols, taken together, help separate effects of voltage and ions on gating vs. permeation. Both protocols were delivered sequentially before, during, and after recovery from Ni^{2+} exposure, to assess current rundown. Two versions of the I-V protocol were run, brief (5 ms) voltage steps from −90 to +200 mV, and longer (40 ms) steps from −90 to 0 mV (+30 mV in 110 mM Ca^{2+}_o or Ba^{2+}_o), since channel activation is not complete in 5 ms at some negative voltages. I-V relations shown in the figures are the peak current (from either the 5 or 40 ms protocol), except in nominally Ca^{2+}_o-free conditions (Fig. 9), where the current at the end of 5-ms steps was used.

Ni^{2+}_o block was described by a simplified Woodhull (1973) model (Khan et al., 2008), with parameters estimated by minimizing the sum of squared errors using the Solver function in Microsoft Excel. Data are shown as mean ± SEM.

Online Supplemental Material

Fig. S1 (available at http://www.jgp.org/cgi/content/full/jgp.200809988/DC1) illustrates our proposal for the mechanism of Ni^{2+} block. Fig. S2 compares one- vs. two-exponential fits to tail

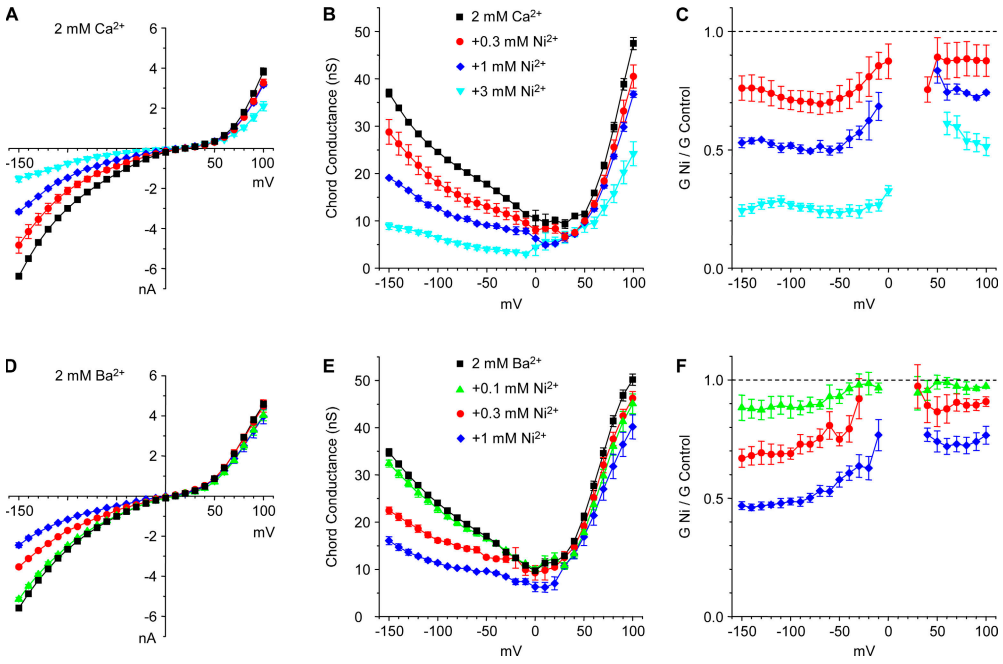

Figure 2. "Instantaneous" inhibition of currents by Ni^{2+}. Initial current amplitudes were measured (see Materials and methods) from the protocol of Fig. 1, in 2 mM Ca^{2+} (A) or 2 mM Ba^{2+} (D). (B and E) Chord conductances, calculated from the data of A and D, respectively. (C and F) The conductance in Ni^{2+} as a fraction of the control conductance in 2 mM Ca^{2+} (C) or 2 mM Ba^{2+} (F). A ratio of 1.0 (dashed lines) represents zero inhibition. Different Ni^{2+} concentrations are indicated by the symbol shapes and color coding defined in B and E in all panels, and also in Figs. 3, 5, and 8 below. In Ca^{2+}, 4 cells were tested in 0.3 mM Ni^{2+}, 3 cells in 1 mM, and 5 cells in 3 mM. In Ba^{2+}, 3 cells were tested in 0.1 mM Ni^{2+}, 4 cells in 0.3 mM, and 4 cells in 1 mM. Note that 3 mM Ni^{2+} was used only in Ca^{2+}, and 0.1 mM Ni^{2+} only in Ba^{2+}.

currents in Ni^{2+}, and supplemental Materials and methods describes how rate constants for Ni^{2+} block were calculated from tail currents. Figs. S3–S7 show additional sample current records in control vs. Ni^{2+}. Figs. S8 and S9 show additional current records and I-V relations for effects of Ni^{2+} on $Ca_V3.2$.

RESULTS

Effect of Ni^{2+} with 2 mM Ca^{2+} or Ba^{2+}

Fig. 1 shows effects of 1 mM Ni^{2+} on $Ca_V3.1$ using the IIV protocol, where channels are first activated by strong depolarization (2 ms at +200 mV) and then repolarized to a wide range of potentials (+100 to −150 mV). Several effects are apparent. First, currents at +200 mV are slower to activate, and are slightly smaller after 2 ms. Second, the "instantaneous" current measured following repolarization is reduced, only slightly at +100 mV, but more substantially at −150 mV. Third, tail currents are faster in Ni^{2+}, especially at the more negative voltages. Fourth, the effect of Ni^{2+} appears to be greater with Ba^{2+} than with Ca^{2+}, especially on the time course of the inward tail currents.

Fig. 2 illustrates effects of Ni^{2+} on the IIV relationships for several concentrations of Ni^{2+}, in 2 mM Ca^{2+} (Fig. 2, A–C) or 2 mM Ba^{2+} (Fig. 2, D–F). Outward currents are reduced only slightly, while inward currents are more sensitive to Ni^{2+}, in a concentration-dependent manner (Fig. 2, A and C). The effects are shown more clearly when currents are converted to chord conductances (Fig. 2, B and E). The voltage dependence of the inhibition is unusual (Fig. 2, C and F), as inhibition seems to depend primarily on the direction of current (inward vs. outward). For example, there is little systematic variation in block between −50 and −150 mV, or from +50 to +100 mV. Furthermore, inhibition is not substantially different between 2 mM Ca^{2+} and Ba^{2+} (compare red and blue symbols, 0.3 mM and 1 mM Ni^{2+}, respectively, in Fig. 2, C and F).

Fig. 3 examines the effects of Ni^{2+} on the kinetics of tail currents, approximated by single exponential fits. In the absence of Ni^{2+}, the time constant reflects a combination of channel deactivation (closing) and inactivation. Voltage-independent inactivation dominates above −50 mV, and voltage-dependent deactivation dominates at more negative voltages (Serrano et al., 1999). Ni^{2+} accelerates tail currents at negative voltages, especially in Ba^{2+} (compare red and blue symbols, 0.3 and 1 mM Ni^{2+}, respectively, in Fig. 3, A and B).

One mechanism by which Ni^{2+} might affect tail kinetics is by voltage- and time-dependent block (Obejero-Paz et al., 2004). We estimated the pseudo first-order rate constant for block by Ni^{2+} (k_B) from either one- or two-exponential fits, as described in supplemental Materials and methods. The calculated rates of Ni^{2+} block are described reasonably well by bimolecular kinetics (straight lines in Fig. 3, C and D), especially with 2 mM Ba^{2+} as the charge carrier, over the range of voltage and $[Ni^{2+}]_o$ where block can be accurately measured.

The calculated rates of Ni^{2+} block exhibit several interesting features. Block was rather strongly voltage dependent,

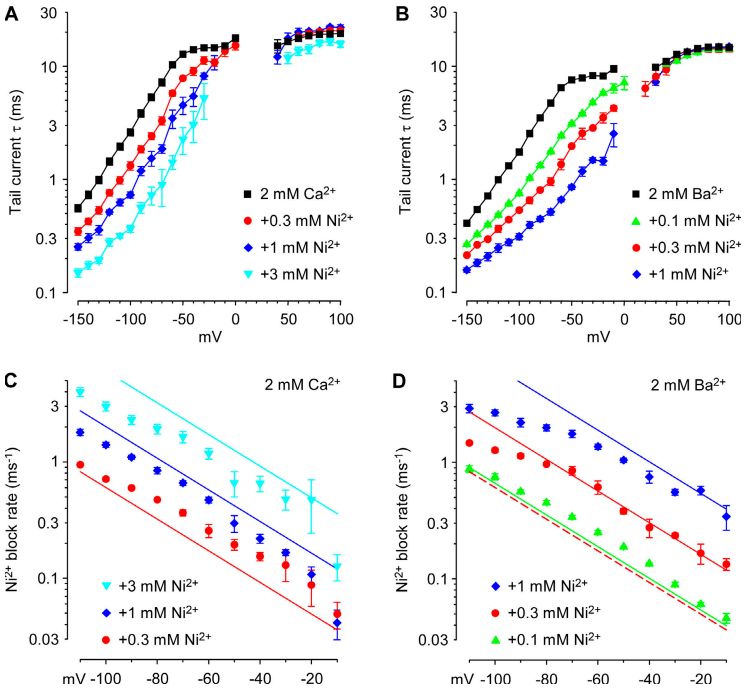

Figure 3. Effects of Ni^{2+} on kinetics of tail currents. Current from the protocol of Fig. 1 were fitted to single exponential functions (see Materials and methods). Time constants are shown in Ca^{2+} (A) and Ba^{2+} (B). The pseudo first-order rate constant for Ni^{2+} block was calculated from fits to two exponentials for Ca^{2+} (C) or one exponential for Ba^{2+} (D), as described in supplemental Materials and methods. Same cells as Fig. 2. The solid lines in C and D are a fit to the rate constants assuming bimolecular kinetics, with equal voltage dependence for Ca^{2+} and Ba^{2+}, from −30 to −70 mV (Ba^{2+}) or −10 to −50 mV (Ca^{2+}), including extrapolation to voltages not included in the fit. The fit to rates for 0.3 mM Ni^{2+} in 2 mM Ca^{2+} is also shown in D, for comparison to the rates in Ba^{2+} (dashed red line).

with rates varying e-fold for 32 mV, corresponding to an apparent electrical distance δ = 0.4 for the transition state for Ni^{2+} entry into the pore. The bimolecular rate constants were several orders of magnitude lower than expected for diffusion-limited entry of Ni^{2+} into the pore, at −80 mV $(1.0 \pm 0.1) \times 10^6\ M^{-1}s^{-1}$ in Ca^{2+} (n = 12, 0.3–3 mM Ni^{2+}) and $(3.1 \pm 0.3) \times 10^6\ M^{-1}s^{-1}$ at −80 mV in Ba^{2+} (n = 11, 0.1–1 mM Ni^{2+}). Note that block was approximately threefold faster in Ba^{2+} than in Ca^{2+}.

Does the faster entry of Ni^{2+} into the pore in Ba^{2+} produce a more potent block? This was examined using I-V relationships, measured as the effect on peak inward or outward current at each voltage (Fig. 4). With this protocol, inward currents were very strongly inhibited in both Ca^{2+} and Ba^{2+}, while outward currents were much less affected (see Fig. S3 for sample current records). Inhibition by Ni^{2+} could be roughly approximated by a Woodhull (1973) model with K_d = 0.2 mM for Ba^{2+} and 0.3 mM for Ca^{2+} (at 0 mV), with weak voltage dependence (e-fold for 64 mV, corresponding to δ = 0.19 for the site of Ni^{2+} block) (Fig. 4, C and F). The Woodhull analysis assumes that the voltage dependence of inhibition by Ni^{2+} results from voltage-dependent pore block, vs. (e.g.) a shift in channel gating to more positive voltages. This issue (and interpretation of δ values) will be considered further in the Discussion.

Estimates of the K_d for block from the IIV protocol (data of Figs. 1 and 2) and the I-V protocol (Fig. 4) are summarized in Fig. 5. With the I-V protocol, Ni^{2+} blocks more strongly in Ba^{2+} than with Ca^{2+} (Fig. 5, open symbols), but the effect is less dramatic than observed for the rate of block by Ni^{2+} (Fig. 3, C vs. D).

Ni^{2+} appears to slow activation of outward currents (Fig. 1 and Fig. S3). One explanation is voltage-dependent relief of resting block by Ni^{2+}, as observed for Y^{3+} (Obejero-Paz et al., 2004). That was examined using current ratios (Ni^{2+}/control) (Fig. 6). The strongest depolarizations produced nearly complete relief of block by 1 mM Ni^{2+} (Fig. 6, A and B), but relief was incomplete even at +200 mV in 3 mM Ni^{2+} (Fig. 6 C).

Fig. 7 shows the analysis of current ratios, measured as in Fig. 6. The extent of Ni^{2+} block remaining after 5 ms of depolarization is shown in Fig. 7 A (in Ca^{2+}) and Fig. 7 D (for Ba^{2+}). The time constant for the current ratios accelerated with depolarization (Fig. 7, B and E). That time constant (τ_{Ni}) should depend on both the on and off rates (Ni^{2+} entry and exit):

$$1/\tau_{Ni} = k_B + k_{-B}, \quad (1)$$

where k_B is the pseudo first-order rate constant for block by Ni^{2+}, and k_{-B} is the rate constant for exit of Ni^{2+} from the pore. Assuming that the Ni^{2+}/control ratio at 5 ms (r_5) (Fig. 7, A and D) reflects steady-state occupancy of Ni^{2+} at each voltage,

$$r_5 = k_{-B}/(k_B + k_{-B}). \quad (2)$$

Eqs. 1 and 2 give two equations for two unknowns (k_B and k_{-B}). Calculated k_{-B} values are shown in Fig. 7 C (in Ca^{2+}) and Fig. 7 F (in Ba^{2+}). Ni^{2+} exit was faster with depolarization, as expected for relief of pore block. The other noteworthy effect is that Ni^{2+} exit was slower in 3 mM Ni^{2+} than in lower concentrations of Ni^{2+} (Fig. 7 C). The final level of inhibition at +50 to +100 mV (Fig. 7, A

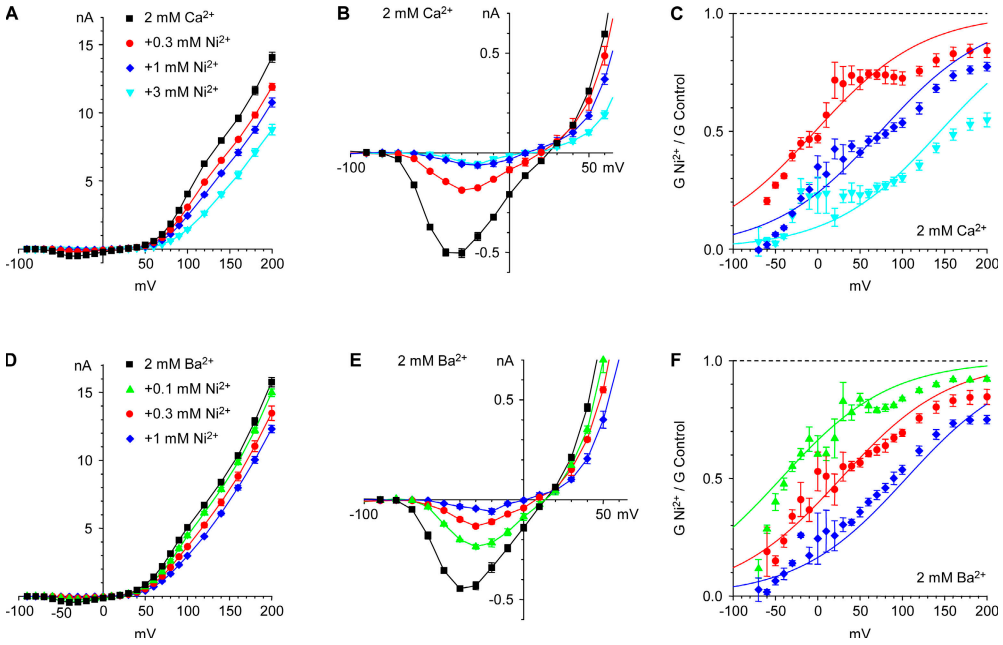

Figure 4. Effects of Ni^{2+} on I-V relations. Currents were measured at the time of maximal current during 5-ms steps. The full voltage range is shown for Ca^{2+} (A) and Ba^{2+} (D); B and E are expanded views to better show inward currents. The ratios of chord conductances (Ni^{2+}/control) are shown for Ca^{2+} (C) and Ba^{2+} (F). The smooth curves in C and F are fits assuming Ni^{2+} blocks the pore by binding at a site in the electrical field of the membrane, and cannot permeate (Woodhull, 1973), with the location of the binding site constrained to be the same for Ca^{2+} and Ba^{2+}. Same cells as Fig. 2.

and D) agrees reasonably well with that measured with the IIV protocol (Fig. 2 C). It is especially noteworthy that strong depolarization did not fully reverse inhibition by 3 mM Ni^{2+} (Fig. 6 C and Fig. 7 A), even though the kinetics were fast ($\tau < 1$ ms, Fig. 7 B). Taken together, these results demonstrate that inhibition of $Ca_V3.1$ by Ni^{2+} cannot be explained by simple voltage-dependent pore block alone. The kinetics of block (from tail currents at negative voltages) and relief of block (from activation at positive voltages) are consistent with a contribution of slow pore block. Slow block can also explain the observation that block is much stronger with the I-V protocol than with the IIV. However, the instantaneous block observed with the IIV and the incomplete relief of block by depolarization to +200 mV in 3 mM Ni^{2+} suggest a faster, lower-affinity process with different ion and voltage dependence (Fig. S1 A). Is the low-affinity site in the pore, or an allosteric site, perhaps related to the site that binds Ni^{2+} with high affinity in $Ca_V3.2$?

Effect of Ni^{2+} with 110 mM Ca^{2+} or Ba^{2+}

We next examined effects of Ni^{2+} at higher concentrations of Ca^{2+} and Ba^{2+} (110 mM). Pore block should be reduced (and slowed) in those conditions, while an allosteric Ni^{2+} site might not be sensitive to Ca^{2+} or Ba^{2+}.

Averaged IIV relationships are shown in Fig. 8 (A and B) and conductance ratios (Ni^{2+}/control) in Fig. 8 C. Chord conductances were reduced by ~15% in Ca^{2+} at all voltages, although measurement was less accurate near the reversal potential. Effects of Ni^{2+} were indistinguishable in Ca^{2+} vs. Ba^{2+} above 0 mV, but peak tail current amplitudes were reduced more strongly in Ba^{2+} at negative voltages. One crucial result is that "instantaneous" block by 3 mM Ni^{2+} is substantially weaker in 110 mM Ca^{2+} (Fig. 8 C) than in 2 mM Ca^{2+} (Fig. 2 C). Sample records are shown in Fig. S4.

Tail currents were accelerated by 3 mM Ni^{2+}, and the effect was clearly greater in 110 mM Ba^{2+} vs. 110 mM Ca^{2+} (Fig. 8, D vs. E). Analyzed on the assumption that the faster tail currents reflect time-dependent block, the rate of block by Ni^{2+} was voltage dependent, 2–3× faster in Ba^{2+} than in Ca^{2+} (Fig. 8 F). From −80 to −10 mV, the rate of block increased e-fold for 35 mV ($\delta = 0.36$). Assuming bimolecular kinetics, the rate of block at −80 mV in 3 mM Ni^{2+} was $(1.1 \pm 0.1) \times 10^5\ M^{-1}s^{-1}$ in Ca^{2+} ($n = 5$) and $(2.7 \pm 0.1) \times 10^5\ M^{-1}s^{-1}$ in Ba^{2+} ($n = 4$). Raising either Ca^{2+} or Ba^{2+} from 2 mM to 110 mM slowed Ni^{2+} entry by ~10-fold.

Effects of 3 mM Ni^{2+} on currents carried by 110 mM Ca^{2+} or Ba^{2+} with the I-V protocol are shown in Fig. 8, G and H (and sample current records, Fig. S5). As with 2 mM Ca^{2+} or Ba^{2+}, Ni^{2+} inhibited inward currents more strongly, and inhibition was stronger in Ba^{2+} than in Ca^{2+}.

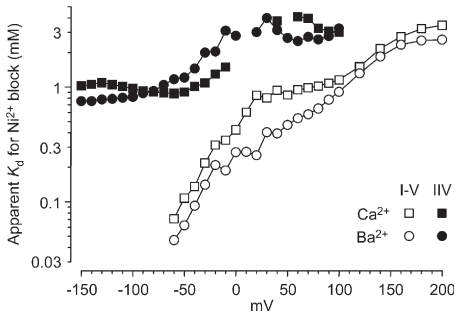

Figure 5. Estimated K_d values for Ni^{2+} block from the IIV and I-V protocols. At each voltage, the Ni^{2+}/control conductance ratios were fitted to the law of mass action. Same cells as Fig. 2.

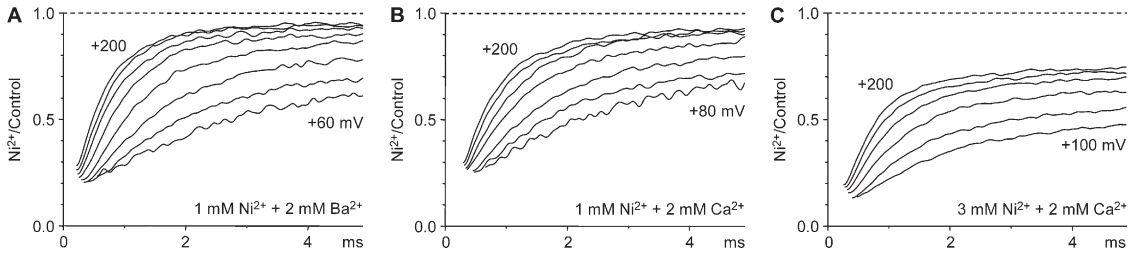

Figure 6. Effects of Ni^{2+} on outward currents during large depolarizations, from the I-V protocol. Records are the ratio of currents recorded in Ni^{2+} to the average control currents, in Ba^{2+} (A) or Ca^{2+} (B and C), for 1 mM Ni^{2+} (A and B) or 3 mM Ni^{2+} (C). Ratios are blanked for 0.3–0.6 ms during the gating current. Voltage steps are in 20-mV increments. 3-kHz Gaussian filter, with 60-Hz noise subtracted for C only. A and B are from the same cells as Figs. 1 and 4, and C is from cell c050929.

However, block was less voltage dependent with 110 mM Ca^{2+} or Ba^{2+} (e-fold for 86 mV, $\delta = 0.15$; K_d at 0 mV = 3.7 mM for Ca^{2+} and 2.2 mM for Ba^{2+}), noting that the data deviate in detail from a Woodhull model. Inhibition of inward currents was stronger with the I-V protocol (Fig. 8 I) than with the IIV protocol (Fig. 8 C), but again the difference was less dramatic than with 2 mM Ca^{2+} or Ba^{2+}.

Effect of Ni^{2+} on Currents Carried by Na^+

The slow rates of Ni^{2+} entry could reflect competitive interactions with permeant divalent cations, but it is also possible that dehydration of Ni^{2+} could be rate limiting for entry into the pore (Winegar et al., 1991). To test this, we recorded currents in the nominal absence of Ca^{2+}_o (and with no extracellular EGTA, which binds Ni^{2+} with high affinity). Contaminating Ca^{2+}_o was estimated to be <3 µM; Khan et al., 2008), and symmetrical 145 mM Na^+ was the charge carrier. With the IIV protocol (Fig. S6 A), inward tail currents were accelerated, and reduced slightly in amplitude, by 30 µM Ni^{2+}. That same concentration of Ni^{2+} produced strong inhibition of inward, but not outward, currents in the I-V protocol (Fig. 9, F–I; Fig. S6 B).

Averaged IIV relationships are shown in Fig. 9 A, for 10, 30, and 100 µM Ni^{2+}. Detailed interpretation is difficult, since even in the control condition there was partial block by Ca^{2+}_o (maximal near −30 mV) and by Mg^{2+}_i (maximal at the most positive voltages), visible in the control chord conductances (Fig. 9 B) (see Khan et al., 2008). Qualitatively, Ni^{2+} block was weak at all voltages at 10 µM, but reached ∼50% inhibition below −100 mV for 100 µM. Block was much stronger with the I-V protocol (Fig. 9, F–I), and could be well described by a Woodhull (1973) model with $K_d = 13$ µM at 0 mV, e-fold for 28 mV ($\delta = 0.45$) (Fig. 9 I).

With Na^+ as charge carrier, tail currents were markedly accelerated by micromolar concentrations of Ni^{2+} (Fig. 9 D and Fig. S5). Ni^{2+} block was voltage and concentration dependent (Fig. 9 E). At −80 mV, the bimolecular block rate was $(3.0 \pm 0.3) \times 10^7\ M^{-1}s^{-1}$ ($n = 12$, 10–100 µM Ni^{2+}). The rate of block, fitted from −50 to −100 mV, varied e-fold for 78 mV ($\delta = 0.16$).

Fig. 10 summarizes the bimolecular rate constants for Ni^{2+} block in the ionic conditions examined in this study. The rate of Ni^{2+} entry varied by >1,000-fold, from $(4.8 \pm 0.3) \times 10^7\ M^{-1}s^{-1}$ (nominally Ca^{2+} free, −120 mV) to $(3.1 \pm 0.2) \times 10^4\ M^{-1}s^{-1}$ (110 mM Ca^{2+}, −20 mV).

Inhibition of $Ca_V3.2$ by Ni^{2+}

Fig. 11 demonstrates that high-affinity inhibition of $Ca_V3.2$ by 20 µM Ni^{2+} does not exhibit the key kinetic

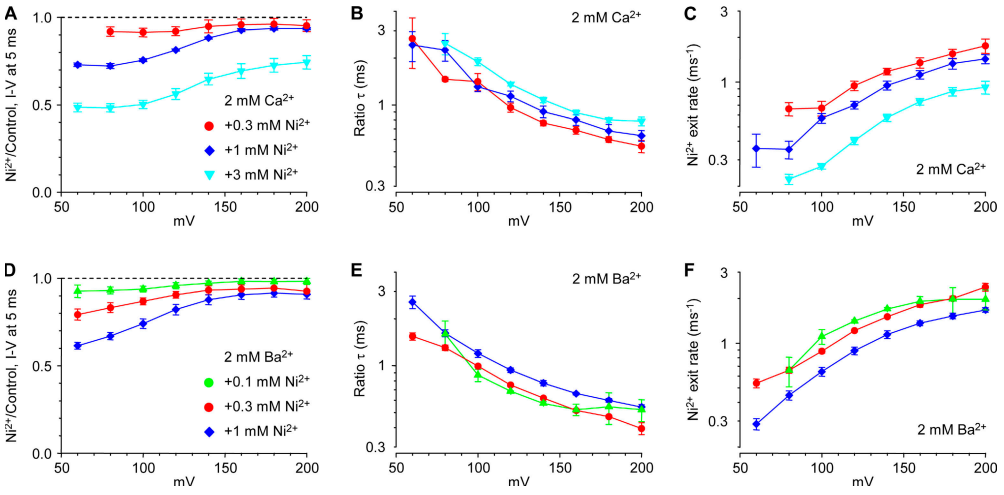

Figure 7. Analysis of Ni^{2+} effects on current ratios during large depolarizations. Current ratios were calculated as in Fig. 6, for the same cells as Fig. 2. Ratios were measured at the end of 5-ms depolarizations in Ca^{2+} (A) and Ba^{2+} (D). Time constants, from single exponential fits to current ratios in Ca^{2+} (B) or Ba^{2+} (E). Rate constants for relief of block by Ni^{2+}, calculated from the fractional block (A and D) and time constants (B and E), from Eqs. 2 and 3, in Ca^{2+} (C) and Ba^{2+} (F).

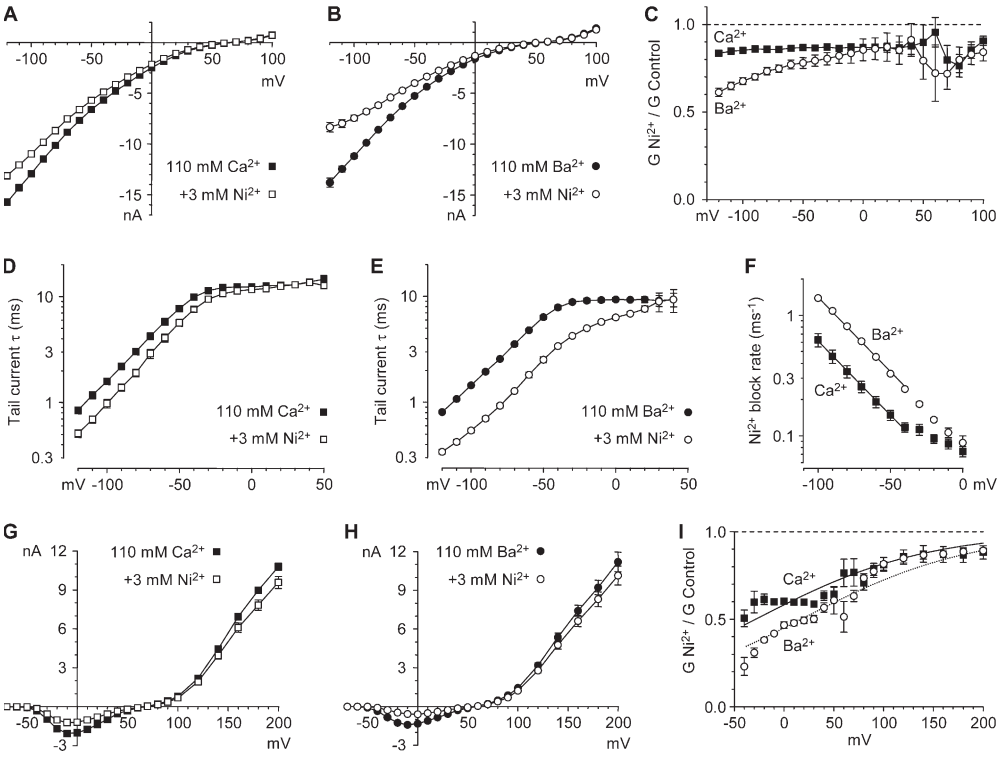

Figure 8. Effects of 3 mM Ni^{2+}, with 110 mM Ca^{2+} or Ba^{2+}. (A and B) Inhibition of IIV currents by Ni^{2+} in Ca^{2+} (A) and Ba^{2+} (B). (C) Inhibition of chord conductances by Ni^{2+}, calculated from the data of A and B. (D and E) Effects of Ni^{2+} on tail current time constants in Ca^{2+} (D) and Ba^{2+} (E). (F) Pseudo first-order rate constants for Ni^{2+} block, calculated from biexponential fits. (G and H) Effects of 3 mM Ni^{2+} on I-V relationships in 110 mM Ca^{2+} (G) and 110 mM Ba^{2+} (H). (I) Effect of Ni^{2+} on chord conductances, from the data of G and I. Smooth curves are Woodhull (1973) fits to data in Ca^{2+} (solid curve) and Ba^{2+} (dotted curve), constrained to have the same voltage dependence (see text for parameters). $n = 5$ (Ca^{2+}), $n = 4$ (Ba^{2+}).

signatures of pore block. Inhibition of $Ca_V3.2$ was nearly independent of voltage over a 350-mV range, and was comparable with the I-V and IIV protocols (Fig. 11, D and E; Fig. S8). Inhibition was not any stronger in 2 mM Ba^{2+} than in Ca^{2+} (Fig. 11, B and C; Fig. S9). There was little effect on the kinetics of tail currents (Fig. 11, F and G); tails were ~20% faster in Ni^{2+} with Ba^{2+} (P = 0.02–0.04 from −80 to −120 mV), possibly indicating a small amount of slow pore block. These results suggest that the kinetic and molecular mechanisms of Ni^{2+} action are fundamentally different for high-affinity inhibition of $Ca_V3.2$, vs. pore block of $Ca_V3.1$.

DISCUSSION

We propose that Ni^{2+} blocks the $Ca_V3.1$ pore at two sites, a relatively superficial low affinity site, and a site deeper within the pore where Ni^{2+} entry is strongly affected by permeant ions (Fig. S1 B). We will first describe how this hypothesis can explain the major features of our results, as well as a substantial number of subtle features. We next consider alternative interpretations, and relate our findings to previous views of Ni^{2+} action on calcium channels.

Two sites for Ni^{2+} Block in the Permeation Pathway of $Ca_V3.1$

Ni^{2+} inhibited currents measured "instantaneously" following strong depolarization. This suggests a site accessible to Ni^{2+} at near the diffusion-limited rate. However, this component of Ni^{2+} block was low affinity, with K_d = 1–3 mM (in 2 mM Ca^{2+} or Ba^{2+}). Fast block had a weak voltage dependence, suggestive of a primary dependence on the direction of current flow (Fig. 2, C and F). Fast block was similar with Ca^{2+} or Ba^{2+} as the charge carrier, but was reduced in 110 mM Ca^{2+} or Ba^{2+} (Fig. 8 C). The effect of high Ca^{2+} or Ba^{2+}, and the voltage or current dependence, suggests that this site is in the ion permeation pathway (as opposed to a completely extracellular site that affects ion flow allosterically). This is supported by the observation that relief of slow block is inhibited by Ni^{2+} at the high concentrations that produce significant fast block (Fig. 7 C), suggesting a weak "lock-in" effect. That effect should be weak, since the "steady-state" outward current is inhibited by <50% at >+150 mV in 3 mM Ni^{2+} (Fig. 6 C), implying <50% occupancy of the fast block site.

The most plausible location for the fast block site is therefore near the outer end of the permeation pathway, perhaps in an outer vestibule, which Ni^{2+} might be able to access readily (perhaps even without dehydrating). If that site is outside the electrical field of the membrane, Ni^{2+} occupancy would not be directly voltage-dependent, but it seems plausible that an outward current could relieve Ni^{2+} block at this superficial site.

Slow block by Ni^{2+} shares several properties of block by other di- and trivalent cations, but there are interesting differences as well. Block is relieved by strong depolarization, as observed for Ca^{2+} (Lux et al., 1990), Mg^{2+} (Serrano et al., 2000), and Y^{3+} (Obejero-Paz et al., 2004). The rate of Ni^{2+} entry is voltage dependent, and is much

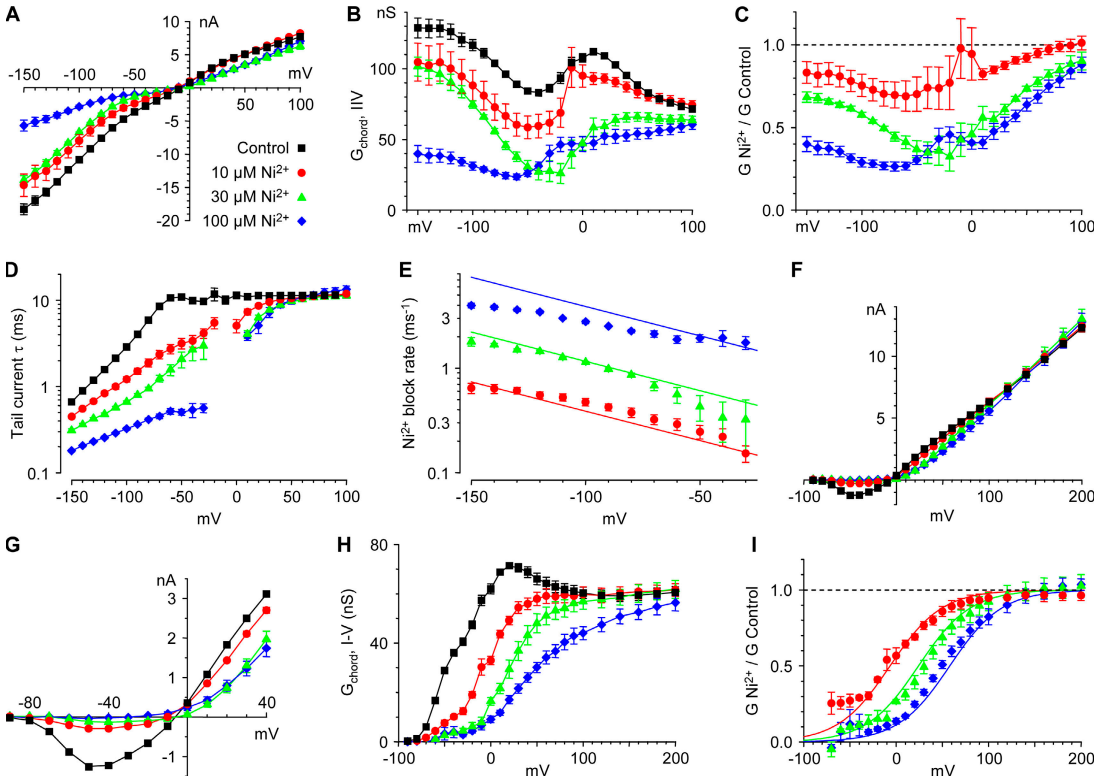

Figure 9. Effects of Ni^{2+} on currents carried by Na^{+}. (A) IIV relations, (B) chord conductances, and (C) inhibition by Ni^{2+}, as conductance ratios (Ni^{2+}/control). (D) Effects of Ni^{2+} on IIV tail currents carried by Na^{+}, from single exponential fits. (E) Pseudo first-order rate constants for Ni^{2+} block, calculated from single exponential fits. (F) I-V relations, (G) I-V relations on an expanded scale, (H) chord conductances, and (I) inhibition by Ni^{2+}, as conductance ratios (Ni^{2+}/control). The smooth curves in I are the best fit to a Woodhull (1973) model. Symbols and color coding in A apply to all panels in this figure. $n = 6$ (10 μM Ni^{2+}) or $n = 4$ (30 μM Ni^{2+} and 100 μM Ni^{2+}), except $n = 5$ in 10 μM Ni^{2+} and $n = 3$ in 30 μM Ni^{2+} for D and E.

slower with Ca^{2+} than with Ba^{2+}, as observed for block of closed channels by Y^{3+}. However, the apparent electrical distance (δ) is 0.4, vs. 0.1 for Y^{3+} (Obejero-Paz et al., 2004), in 2 mM Ca^{2+}. Note that this δ value, estimated from the entry rate, is the apparent electrical distance

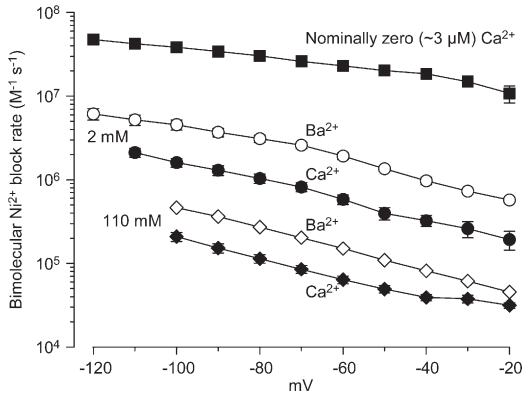

Figure 10. Bimolecular rate constants for Ni^{2+} block in different ionic conditions, from IIV protocols. Values include data in all concentrations of Ni^{2+}, $n = 12$ (nominally Ca^{2+} free), $n = 12$ (2 mM Ca^{2+}), $n = 11$ (2 mM Ba^{2+}), $n = 5$ (110 mM Ca^{2+}, all at 3 mM Ni^{2+}), and $n = 4$ (110 mM Ba^{2+}, all at 3 mM Ni^{2+}).

to the energy barrier that limits Ni^{2+} entry, not the distance to the actual binding site. Curiously, δ varied with ionic conditions (see below). The bimolecular rates for Ni^{2+} entry are much lower than for Ca^{2+} (3×10^{8} $M^{-1}s^{-1}$ near −60 mV; Khan et al., 2008) or Y^{3+} (10^{9} $M^{-1}s^{-1}$ at −80 mV; Obejero-Paz et al., 2004).

Taken together, the most plausible site for slow block by Ni^{2+} is the selectivity filter for Ca^{2+}. Ni^{2+} appears to have considerable difficulty in entering this site, even though it is thought to be physically near the extracellular side of the pore. This may involve both slow dehydration and competitive ion–ion interactions. These two factors may be related, since compared with many other di- and trivalent cations, Ni^{2+} entry might require more complete replacement of waters of hydration with the side chains of the glutamate and aspartate residues of a Ca_V3 selectivity filter, which could increase the ability of ions within the pore to prevent Ni^{2+} entry. Perhaps some ions (e.g., Y^{3+}) can aggressively push any competing Ca^{2+} or Ba^{2+} ions through the pore, while Ni^{2+} must wait patiently in the low-affinity fast-block site until Ca^{2+} or Ba^{2+} ions permeate. In that view, most ions pass quickly by the site where Ni^{2+} occupancy produces a fast block. That could explain the

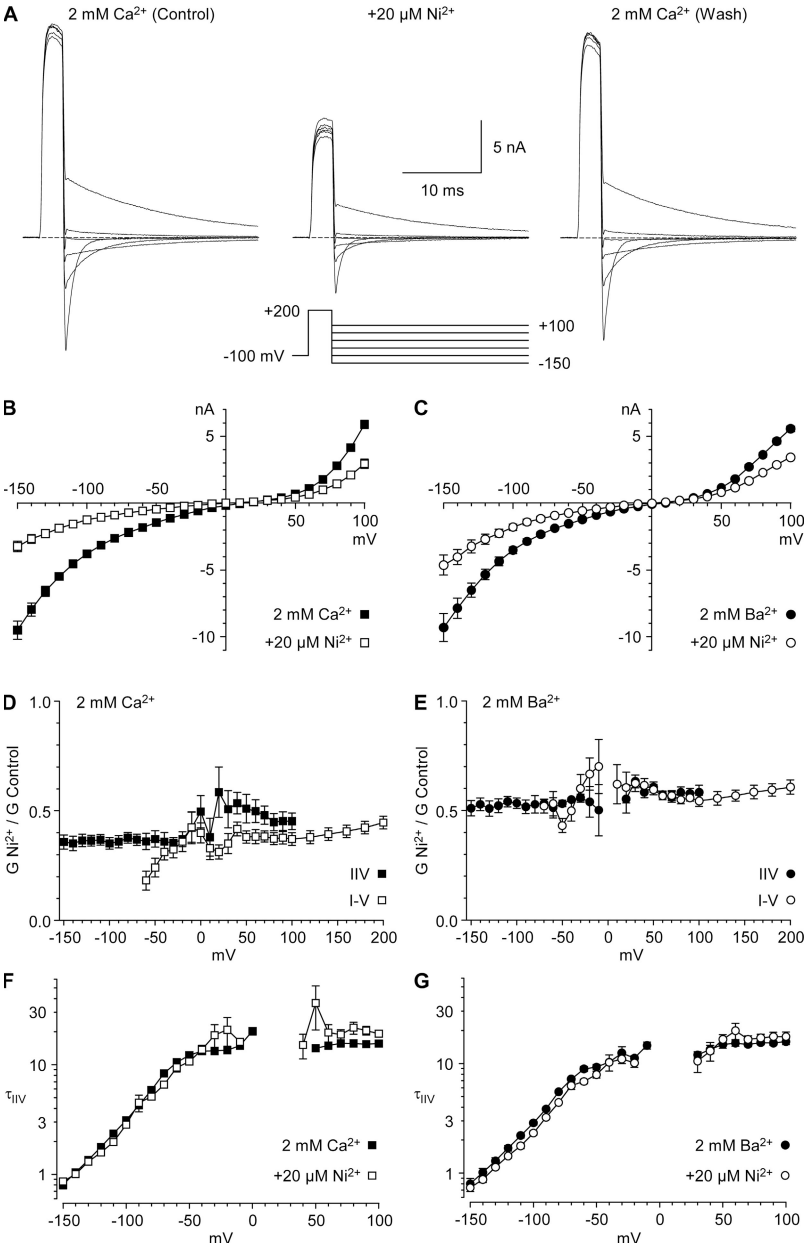

Figure 11. Inhibition of $Ca_V3.2$ by 20 μM Ni^{2+}. (A) Sample currents with the IIV protocol. Cell d080508, 3-kHz Gaussian filter. (B and C) IIV relationships for inhibition by Ni^{2+} in 2 mM Ca^{2+} ($n = 7$) and 2 mM Ba^{2+} ($n = 4$). Prepulses to +60 mV were 2 ms or 3 ms in different cells. (D and E) Ni^{2+}/control ratios, calculated from chord conductances, from IIV and I-V protocols (see Figs. S8 and S9). (F and G) Time constants from the IIV protocol.

lack of Ca^{2+}–Ba^{2+} selectivity for effects on fast block by Ni^{2+}.

Why is the δ for Ni^{2+} entry so large, and so ion dependent? Those two features together suggest that the large δ is a consequence of strong interactions with other ions within the pore, rather than an accurate measure of an electrical location within the pore. The ion dependence predicts that the δ for Ni^{2+} entry should approach the "true" value in the absence of competition, which would explain the observation that δ is lower in Na^+ (0.16, vs. ~0.4 in 2–110 mM Ca^{2+} or Ba^{2+}).

It is noteworthy that the extent of block, measured from I-V relations, was less ion dependent than the rate of block. Furthermore, the apparent voltage dependence of block depended in the opposite direction on ion concentration, with δ = 0.45 in Na^+, δ = 0.19 in 2 mM Ca^{2+} or Ba^{2+}, and δ = 0.15 in 110 mM Ca^{2+} or Ba^{2+}. This can be explained in part by the low-affinity Ni^{2+}-binding site, which is relatively insensitive to ionic conditions and to voltage. That site would make the largest contribution to the net block by Ni^{2+} when "high-affinity" slow block is the weakest (in high Ca^{2+}). In addition, the measured δ could be in error if Ni^{2+} affects gating, or if slow Ni^{2+} block has not reached steady state at the time of peak current.

This two-site model for pore block by Ni^{2+} provides an attractive qualitative explanation for the behavior of Ni^{2+} block under a variety of ionic conditions, and a wide range of voltages. However, we are well aware that this will need to be confirmed by molecularly based modeling of ion permeation in calcium channels, at a

sufficient level of detail to account for the complex organometallic chemistry of Ni^{2+} ions.

The Ni^{2+} entry rate was sensitive to the identity of the permeant divalent cation (Ca^{2+} vs. Ba^{2+}), even at 110 mM concentrations where flux through the pore is saturated (Khan et al., 2008). It is often assumed that saturation of flux implies saturation of binding site(s) within the pore, but that is not necessarily true.

Alternative Interpretations of Ni^{2+} Action

As for any pharmacological agent, there are several possible mechanisms by which an ion such as Ni^{2+} can affect the behavior of a voltage-dependent ion channel, including pore block, shifts in gating by screening or binding to surface charge, and allosteric modulation by binding to extra-pore sites.

There is good reason to expect that Ni^{2+} will shift channel activation to more positive potentials, at least in part by a surface charge mechanism. Effects of three other divalent cations (Ca^{2+}, Ba^{2+}, and Mg^{2+}) on gating were well described by screening a surface charge of 1 e^- per 98 $Å^2$, which predicts (e.g.) that addition of 1 mM divalent cation to 2 mM Ca^{2+} or Ba^{2+} would shift channel activation by ~3 mV. It is possible that Ni^{2+} affects surface charge more strongly than Ca^{2+}, Ba^{2+}, and Mg^{2+}; for example, Fe^{2+} and Mn^{2+} shift gating as expected for both screening and low-affinity binding to surface charge (Lopin, K.V., I.P. Gray, C.A. Obejero-Paz, and S.W. Jones. 2007. Biophysical Society meeting. Abstract 2867; Jamieson, Q., C.A. Obejero-Paz, and S.W. Jones. 2008. Biophysical Society meeting. Abstract 3129).

The effect of Ni^{2+} on tail kinetics is in the direction expected for a surface charge effect: that is, faster tail currents (measured at a particular voltage) could in principle result from a positive shift along the voltage axis. However, where the effect of Ni^{2+} on tail current time constants was the strongest (2 mM Ba^{2+}, Fig. 3 B; nominally Ca^{2+} free, Fig. 9 D), the effect was not a pure parallel shift along the voltage axis. Furthermore, the effect of Ni^{2+} to speed tail currents more profoundly in Ba^{2+} vs. Ca^{2+} would not be expected from a surface charge mechanism. Finally, this interpretation would imply that it is merely coincidental that the effect on tail kinetics is well approximated by bimolecular kinetics with a voltage-dependent rate for Ni^{2+} block (Fig. 3, C and D, Fig. 8 F, and Fig. 9 E). Thus, we conclude that Ni^{2+} speeds tail currents primarily by voltage- and time-dependent channel block, not by effects on channel gating.

Several figures in this paper present the fractional inhibition by Ni^{2+} of the peak current measured from I-V relationships (Fig. 4, C and F, Fig. 8 I, and Fig. 9 I). Inhibition can result from voltage-dependent block by Ni^{2+} within the ion permeation pathway, but a positive shift in channel activation would also lead to a voltage-dependent reduction in current amplitudes. This complicates interpretation of the Woodhull (1973) fits to the data from the I-V protocol. Specifically, if Ni^{2+} shifts activation to more positive voltages (even by a few mV), inhibition at more negative voltages would reflect a combination of pore block and a reduction in the probability that a channel is open. It is important to recognize that a positive shift in the I-V curve (or derived measures such as the G-V) could result either from a true shift in channel activation, or from voltage-dependent block. For a fast blocker (e.g., Mg^{2+}) pore block can be measured as a reduction in the IIV, and shifts in gating from the I-V/IIV ratio ($P_{O,r}$), but separation of the two effects is difficult for a slow blocker such as Ni^{2+}. If block is very slow, the block observed at the time of peak current with the I-V protocol may not fully reflect steady-state block, as noted previously for other channel blockers (Thévenod and Jones, 1992; Block et al., 1998; Babich et al., 2007).

In principle, surface charges could also affect ion permeation, if the charges are close enough to the permeation pathway to affect the local concentration of permeating and blocking cations. However, this effect appears to be minimal for voltage-dependent calcium channels (Kuo and Hess, 1992; Block et al., 1998).

One possible explanation of the low-affinity inhibition by Ni^{2+} of the IIV relationship is that $Ca_V3.1$ retains a low-affinity extracellular site for Ni^{2+} block, homologous to the high-affinity site in $Ca_V3.2$. Perhaps Ni^{2+} traps a voltage sensor in the "down" position, analogous to voltage sensor toxins (Li-Smerin and Swartz, 1998; McDonough, 2007). That could slow activation, and/or keep some channels from opening at all. We cannot fully exclude this, but that mechanism would not easily explain the reduced fast block in 110 mM Ca^{2+} or Ba^{2+}. Furthermore, concentrations of Ni^{2+} that occupy that low-affinity site "lock in" Ni^{2+} block at the deep pore site, suggesting a more direct interaction (which we propose to be at the extracellular side of the permeation pathway). Note also that high-affinity inhibition of $Ca_V3.2$ is not reversed even by depolarization to +200 mV (Fig. 11), consistent with simple voltage-independent inhibition (Diaz et al., 2005; Kang et al., 2005).

This study illustrates how the basic I-V and IIV protocols, combined with an analysis of ion dependence, can go a long way toward determining the mechanisms of action of an ion such as Ni^{2+} on a calcium channel. A discrepancy between the extent of inhibition measured from the I-V and IIV protocols can be explained either by time-dependent block, or by modified channel activation. Acceleration of tail currents may result either from time-dependent open-channel block or from a shift in activation, but differential effects on tail kinetics in Ca^{2+} vs. Ba^{2+} strongly suggest a pore block mechanism. That is especially true for $Ca_V3.1$, where changes in Ca^{2+} and Ba^{2+} concentration shift the voltage dependence of

gating in the same manner, implying similar "surface charge" effects of Ca^{2+} and Ba^{2+} on channel activation. Analysis of tail current acceleration in terms of pore block can test that hypothesis by comparison to expectations for a bimolecular reaction, with voltage-dependent rates. Conversely, analysis based solely on effects on I-V relationships may not be sufficient for mechanistic analysis. For example, Lacinova et al. (2000) concluded that Ni^{2+} modified activation kinetics for $Ca_V3.1$, by slowing channel deactivation (more strongly in 20 mM Ba^{2+} vs. Ca^{2+}). Their experimental results are consistent with ours, but we conclude instead that Ni^{2+} accelerates tail currents primarily by time- and voltage-dependent block, vs. a true modulation of the kinetics of channel closing.

Comparison to Previous Studies of Ni^{2+} Block of Calcium Channels

We propose that Ni^{2+} block of $Ca_V3.1$ involves a low affinity site with rapid kinetics, and a high affinity site within the "deep" pore. This agrees quite well with single-channel data on Ni^{2+} block of L-type calcium channels (Winegar et al., 1991), where Ni^{2+} not only reduced the apparent single channel conductance, but also produced discrete blocking events. The rate for discrete block of L channels by Ni^{2+} was also quite slow, $6 \times 10^4\ M^{-1}s^{-1}$ at 0 mV in 110 mM Ba^{2+} (Winegar et al., 1991), compared with $3 \times 10^4\ M^{-1}s^{-1}$ for $Ca_V3.1$ (from Fig. 8 F). In addition, the rates of block and relief of block both increased with hyperpolarization (Winegar et al., 1991), consistent with our observation that the rate of block by Ni^{2+} was more voltage dependent than the steady-state block (which depends on the off/on rate ratio). We do not have direct measurements of the exit rate, but note that an exit rate that increases with hyperpolarization suggests that Ni^{2+} can exit the pore to the intracellular site (i.e., Ni^{2+} is a weakly permeant ion).

Many previous studies, on T channels (Lee et al., 1999; Kang et al., 2005) and other calcium channels (Zamponi et al., 1996; McFarlane and Gilly, 1998; Magistretti et al., 2001), concluded that Ni^{2+} modified channel gating, most likely by an extra-pore site. Our results do not provide compelling evidence for such an effect for $Ca_V3.1$. This is consistent with the interpretation that the high-affinity site near the extracellular side of S4 in $Ca_V3.2$ is essentially absent in $Ca_V3.1$ (Kang et al., 2005).

We thank Dr. Ed Perez-Reyes for the gift of cells stably transfected with $Ca_V3.1$, and for a plasmid encoding $Ca_V3.2$.

This work was supported by National Institutes of Health grant NS24771 to S.W. Jones.

Olaf S. Andersen served as editor.

Submitted: 14 February 2008
Accepted: 26 June 2008

REFERENCES

Almers, W., E.W. McCleskey, and P.T. Palade. 1984. A non-selective cation conductance in frog muscle membrane blocked by micromolar external calcium ions. *J. Physiol.* 353:565–583.

Babich, O., J. Reeves, and R. Shirokov. 2007. Block of $Ca_V1.2$ channels by Gd^{3+} reveals preopening transitions in the selectivity filter. *J. Gen. Physiol.* 129:461–475.

Block, B.M., W.C. Stacey, and S.W. Jones. 1998. Surface charge and lanthanum block of calcium current in bullfrog sympathetic neurons. *Biophys. J.* 74:2278–2284.

Diaz, D., R. Bartolo, D.M. Delgadillo, F. Higueldo, and J.C. Gomora. 2005. Contrasting effects of Cd^{2+} and Co^{2+} on the blocking/unblocking of human Ca_V3 channels. *J. Membr. Biol.* 207:91–105.

Hagiwara, N., H. Irisawa, and M. Kameyama. 1988. Contribution of two types of calcium currents to the pacemaker potentials of rabbit sino-atrial node cells. *J. Physiol.* 395:233–253.

Hess, P., and R.W. Tsien. 1984. Mechanism of ion permeation through calcium channels. *Nature.* 309:453–456.

Kang, H.W., J.Y. Park, S.W. Jeong, J.A. Kim, H.J. Moon, E. Perez-Reyes, and J.H. Lee. 2005. A molecular determinant of nickel inhibition in $Ca_V3.2$ T-type calcium channels. *J. Biol. Chem.* 281:4823–4830.

Khan, N., I.P. Gray, C.A. Obejero-Paz, and S.W. Jones. 2008. Permeation and gating in $Ca_V3.1$ (α1G) T-type calcium channels. Effects of Ca^{2+}, Ba^{2+}, Mg^{2+}, and Na^+. *J. Gen. Physiol.* 132:223–238.

Kuo, C.C., and P. Hess. 1992. A functional view of the entrances of L-type Ca^{2+} channels: estimates of the size and surface potential at the pore mouths. *Neuron.* 9:515–526.

Lacinova, L., N. Klugbauer, and F. Hofmann. 2000. Regulation of the calcium channel α_{1G} subunit by divalent cations and organic blockers. *Neuropharmacology.* 39:1254–1266.

Lee, J.H., J.C. Gomora, L.L. Cribbs, and E. Perez-Reyes. 1999. Nickel block of three cloned T-type calcium channels: low concentrations selectively block α1H. *Biophys. J.* 77:3034–3042.

Li-Smerin, Y., and K.J. Swartz. 1998. Gating modifier toxins reveal a conserved structural motif in voltage-gated Ca^{2+} and K^+ channels. *Proc. Natl. Acad. Sci. USA.* 95:8585–8589.

Lux, H.D., E. Carbone, and H. Zucker. 1990. Na^+ currents through low-voltage-activated Ca^{2+} channels of chick sensory neurones: block by external Ca^{2+} and Mg^{2+}. *J. Physiol.* 430:159–188.

Magistretti, J., S. Brevi, and M. De Curtis. 2001. Ni^{2+} slows the activation kinetics of high-voltage-activated Ca^{2+} currents in cortical neurons: evidence for a mechanism of action independent of channel-pore block. *J. Membr. Biol.* 179:243–262.

McDonough, S.I. 2007. Gating modifier toxins of voltage-gated calcium channels. *Toxicon.* 49:202–212.

McFarlane, M.B., and W.F. Gilly. 1998. State-dependent nickel block of a high-voltage-activated neuronal calcium channel. *J. Neurophysiol.* 80:1678–1685.

Narahashi, T., A. Tsunoo, and M. Yoshii. 1987. Characterization of two types of calcium channels in mouse neuroblastoma cells. *J. Physiol.* 383:231–249.

Obejero-Paz, C.A., I.P. Gray, and S.W. Jones. 2004. Y^{3+} block demonstrates an intracellular activation gate for the α1G T-type Ca^{2+} channel. *J. Gen. Physiol.* 124:631–640.

Serrano, J.R., E. Perez-Reyes, and S.W. Jones. 1999. State-dependent inactivation of the α1G T-type calcium channel. *J. Gen. Physiol.* 114:185–201.

Serrano, J.R., S.R. Dashti, E. Perez-Reyes, and S.W. Jones. 2000. Mg^{2+} block unmasks Ca^{2+}/Ba^{2+} selectivity of α1G T-type calcium channels. *Biophys. J.* 79:3052–3062.

Soong, T.W., A. Stea, C.D. Hodson, S.J. Dubel, S.R. Vincent, and T.P. Snutch. 1993. Structure and functional expression of a

member of the low voltage- activated calcium channel family. *Science*. 260:1133–1136.

Thévenod, F., and S.W. Jones. 1992. Cadmium block of calcium current in frog sympathetic neurons. *Biophys. J.* 63:162–168.

Winegar, B.D., R. Kelly, and J.B. Lansman. 1991. Block of current through single calcium channels by Fe, Co, and Ni. Location of the transition metal binding site in the pore. *J. Gen. Physiol.* 97:351–367.

Woodhull, A.M. 1973. Ionic blockage of sodium channels in nerve. *J. Gen. Physiol.* 61:687–708.

Yang, J., P.T. Ellinor, W.A. Sather, J.F. Zhang, and R.W. Tsien. 1993. Molecular determinants of Ca^{2+} selectivity and ion permeation in L-type Ca^{2+} channels. *Nature*. 366:158–161.

Zamponi, G.W., E. Bourinet, and T.P. Snutch. 1996. Nickel block of a family of neuronal calcium channels: subtype- and subunit-dependent action at multiple sites. *J. Membr. Biol.* 151:77–90.